Electronic Supplementary Material (ESI) for Environmental Science: Nano.

Supporting Information

Revealing charge transfer mechanism and assessing products toxicity in 2D/1D $Bi_2O_2CO_3/Bi_8(CrO_4)O_{11}$ heterostructure system

1. Experimental procedure

1.1. Preparation of catalysts

1.1.1. Preparation of $Bi_8(CrO_4)O_{11}$ (BCrO)

First, 2×10^{-3} mol (0.632 g) $NaBiO_3 \cdot 2H_2O$ was ultrasonically dispersed in 80 mL deionized water for 10 min, and then 7.35 mL, 25 mmol L^{-1} $Cr(NO_3)_3$ aqueous solution was added under vigorous stirring for 1 h. After that, it was put into a 100 mL polytetrafluoroethylene reaction kettle and kept at 180 °C for 6 h. When cooled to room temperature, it was washed alternately with water and alcohol for several times, vacuum dried at 70 °C overnight, and $Bi_8(CrO_4)O_{11}$ (BCrO) was collected.

1.1.2. Preparation of C_3N_4 (CN)

10 g urea was calcined in a muffle furnace at 500 ℃ for 2 h; then heated to 550 ℃ for another 2 h with 3 ℃ min^{-1}. The obtained sample was named as g-C_3N_4 (CN).

1.1.3. Preparation of $Bi_2O_2CO_3$ (BOC)

Typically, 0.632 g of $NaBiO_3 \cdot 2H_2O$ was added to 20 mL of dispersed g-C_3N_4 (0.12 g, ultrasonic for 60 min) solution with ultrasonic for 10 min, and then stirred for 60 min. It was kept at 180 °C for 6 h. When cooled to room temperature, it was washed alternately with water and alcohol for several times, dried under vacuum at 70 °C overnight, and $Bi_2O_2CO_3$ (BOC) was collected.

1.1.4. Preparation of $Bi_2O_2CO_3/Bi_8(CrO_4)O_{11}$ heterojunctions (BOC/BCrO)

Different ratios of $Bi_2O_2CO_3/Bi_8(CrO_4)O_{11}$ (BOC/BCrO) heterojunctions were synthesized by controlling the mass of g-C_3N_4 (carbon source). The well dispersed g-C_3N_4 was dropped into $NaBiO_3 \cdot 2H_2O$ solution, with the total volume of 80 mL. Then, 7.35 mL of 25 mmol L^{-1} $Cr(NO_3)_3$ aqueous solution was added to the above solution and stirred for 60 min. After that, put it into a 100 mL polytetrafluoroethylene reactor

and keep it at 180 °C for 6 h. When cooled to room temperature, it was washed alternately with water and alcohol for several times, dried under vacuum at 70 °C for 10 h. When the added amount of g-C_3N_4 was controlled at 0.0036, 0.018, 0.072 and 0.18 g, 1%, 5%, 20% and 50% BOC/BCrO heterojunctions were obtained, respectively.

1.2. Characterization

The crystallographic structures of samples were analyzed by powder X-ray diffraction (XRD) using a Bruker D8 advance X-ray diffractometer with Cu Kα radiation (λ = 0.1540 nm) and a scanning speed of 3^o min^{-1}. Fourier transform infrared spectroscopy (FT-IR) was measured on a Nicolet 6700 Thermo Fisher spectrophotometer with a substrate by KBr. The optical properties were characterized by UV-Vis diffuse reflectance spectroscopy (UV-Vis DRS) using a UV-Vis spectrophotometer (Shimadzu UV-2550). Total organic Carbon were checked by Total Organic Carbon analyzer (TOC-2000, Shanghai Metash Instruments Co., Ltd). N_2 physisorption measurements were carried out at 77 K using a Micromeritics Tristar II 3020 surface area analyzer. Multipoint Brunauer-Emmett-Teller (BET) specific surface areas were then determined from the adsorption isotherms. The X-ray photoelectron spectroscopy (XPS) was measured on a Thermo Fischer ESCALAB Xi^+ spectrometer with an Al Kα X-ray beam. The binding energies were corrected regarding the C 1s peak of the surface adventitious carbon at 284.8 eV. Transmission electron microscopy (TEM) and high-resolution transmission electron microscopy (HRTEM) images were performed on a JEM-2100 with an accelerating voltage of 200 kV. Dielectric constant (ε) was measured by Precision Impedance Analyzers 6500B Series. Photoelectrochemical measurements: 5 mg sample was dispersed in 400 μL of deionized water by sonication to get uniform slurry. Then the 20 μL slurry was deposited as a film on a 0.5 cm × 0.5 cm fluorine-doped tin oxide (FTO) conducting glass to obtain the working electrode. After dried at room temperature, the working electrode was obtained. Ag/AgCl as reference electrode, platinum wire as counter electrode. The photocurrent test and flat band potential (M-S plots) was carried out in

a three-electrode system in a 0.2 mol L^{-1} Na_2SO_4 solution. Impedance is carried out in a mixture of 0.1 mol L^{-1} KCl and 0.1 mol L^{-1} $K_3[Fe(CN)_6]$/ $K_4[Fe(CN)_6]$.

1.3. Photocatalytic activity testing

The typical dyes (MB (methylene blue), MO (methyl orange) and RhB (rhodamine b): 10 ppm) and typical antibiotics (BPA (bisphenol A), TC (tetracycline) and NOR (norfloxacin): 20 ppm) were selected as probe to explore the photocatalytic performance of the prepared catalysts. A 300 W Xe lamp was used as the light source. The 50 mg photocatalyst was added into 50 mL solution and stirred for 30 min in the dark to achieve the dynamic equilibrium of adsorption and desorption. 3 mL of mixed suspension was taken out at certain intervals and centrifuged. The supernatants were analyzed by UV-Vis spectrophotometer or liquid chromatography. The degradation efficiency was calculated by $(1-C_t/C_0) \times 100\%$, where C_0 and C_t are the initial and residual concentrations of pollutants, respectively.

1.4. Structure and DFT computational detail

Density functional theory (DFT) calculations for $Bi_2O_2CO_3$ and $Bi_8(CrO_4)O_{11}$ were carried out through the Materials Studio (BIOVIA V2017, American) with the CASTEP mode. The Perdew-Burke-Ernzerhof (PBE) form exchange-correlation functional was used within the generalized gradient approximation (GGA). The structures of the (-202) facet of $Bi_8(CrO_4)O_{11}$ and the (013) facet of $Bi_2O_2CO_3$ are optimized. After geometry optimization, the average potential profile was calculated to acquire the work functions of $Bi_2O_2CO_3$ and $Bi_8(CrO_4)O_{11}$.

For $Bi_2O_2CO_3$: The cutoff energy of 500 eV and the Monkhorst-Pack grids of 17 × 1 × 1 were used. The convergence thresholds for the geometry optimization were set as 1.0×10^{-5} eV/atom for energy and 0.02 eV/Å for maximum force.

For $Bi_8(CrO_4)O_{11}$: The cutoff energy of 500 eV and the Monkhorst-Pack grids of 6 × 6 × 1 were used. The convergence thresholds for the geometry optimization were set as 1.0×10^{-5} eV/atom for energy and 0.02 eV/Å for maximum force.

Table S1. The calculated carrier concentrations of BOC and BCrO.

1000 Hz	$[dU_{FL}/d(1/C^2)]^{-1}$	ε	N_d (cm^{-3})
BOC	8×10^4	253.47	6.96×10^{22}
BCrO	4.68×10^8	399.07	7.53×10^{18}

Table S2. Important parameters of typical semiconductors for BPA degradation

Catalyst	Quality	Concentration; Volume	Time; Degradation	Light source	Refs.
Porous N/S doped carbon embedded with ZnS	10 mg	10 ppm, 50 mL	150 min, 88%	Lab Solar-IIIAG, Perfect light Limited, Beijing	S1
Chitosan supported covalent organic framework	Film containing 5 mg COFs	3 ppm, 60 mL	180 min, 94%	300 W Xe lamp	S2
ZnO-CdO	0.6 g/L	10 ppm, 50 mL	180 min, 98.5%	30 W, 365 nm	S3
$BiOI/Fe_3O_4$ (2:1)	1 g/L	10 ppm,	30 min, 100%	150-W xenon lamp	S4
$Cu\text{-}N/TiO_2$	0.5 g/L	10 ppm, 250 mL	120 min, 42.7%	LED light (λmax = 457 nm)	S5
$BiOCl_{0.75}I_{0.25}/g\text{-}C_3N_4$ on polyolefin polyester fiber (PPF)	0.2 g/L on PPF	10 ppm, 50 mL	60 min, 100%	500 W Xe lamp	S6
$SrTiO_3/BiOI$	1 g/L	10 ppm	90 min, 90%	300 W Xe lamp	S7
$Ag/AgCl/SrTiO_3$	0.05 g	10 ppm, 100 mL	83%, 240 min	300 W Xe lamp	S8
$g\text{-}C_3N_4/Bi_8(CrO_4)O_{11}$	50 mg	20 ppm, 50 mL	20 min, 96%	300 W Xe lamp	This work

Table S3. Germination ratio and shoot length of wheat seedlings treatment by H_2O and 20% BOC/BCrO for seven days.

Criteria	**Germination ratio (%)**	**Mean**	**Shoot length (cm)**	**Mean**
CK-1	94	96±2	9.2±1.06	8.91±0.4
CK-2	98		9.03±1.18	
CK-3	96		8.51±1.4	
Catalyst-1	94	94	8.83±0.94	9.08±0.2
Catalyst-2	94		9.29±1.06	
Catalyst-3	94		9.12±1.67	

Note:

CK means treated by H_2O.

Catalyst means treated by 20% BOC/BCrO heterojunction.

The numbers 1, 2, 3 represent parallel experiments.

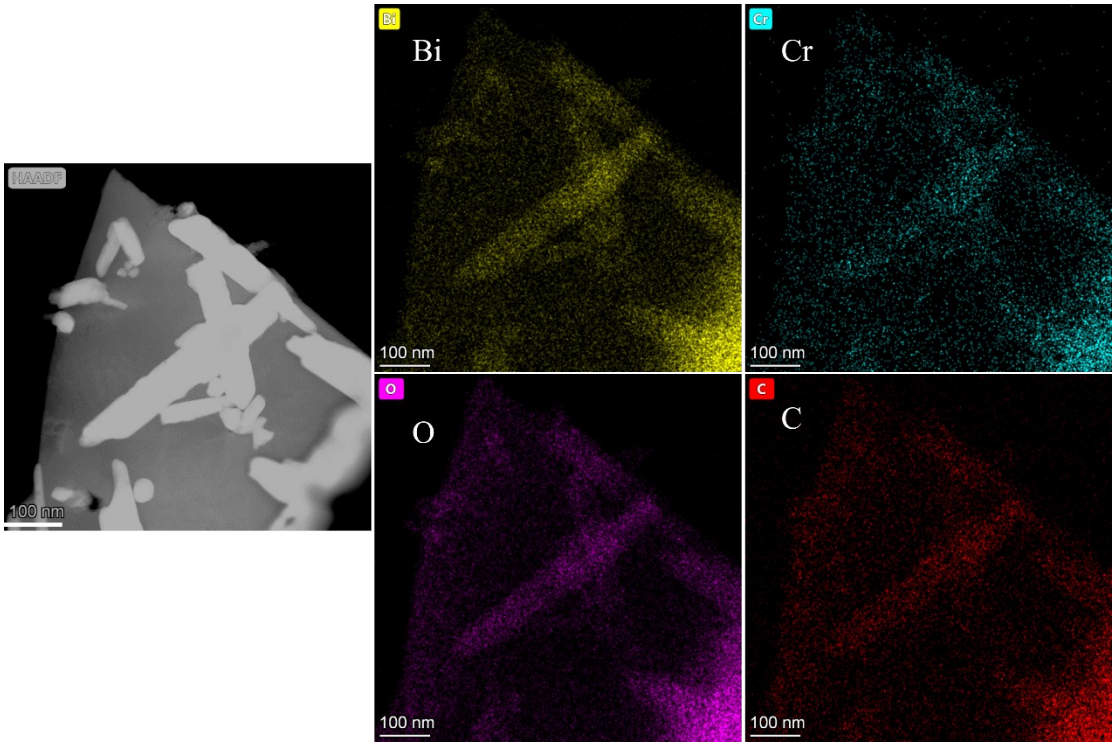

Fig. S1. TEM image of 20% BOC/BCrO and the corresponding elemental mapping of Bi, Cr, O and C.

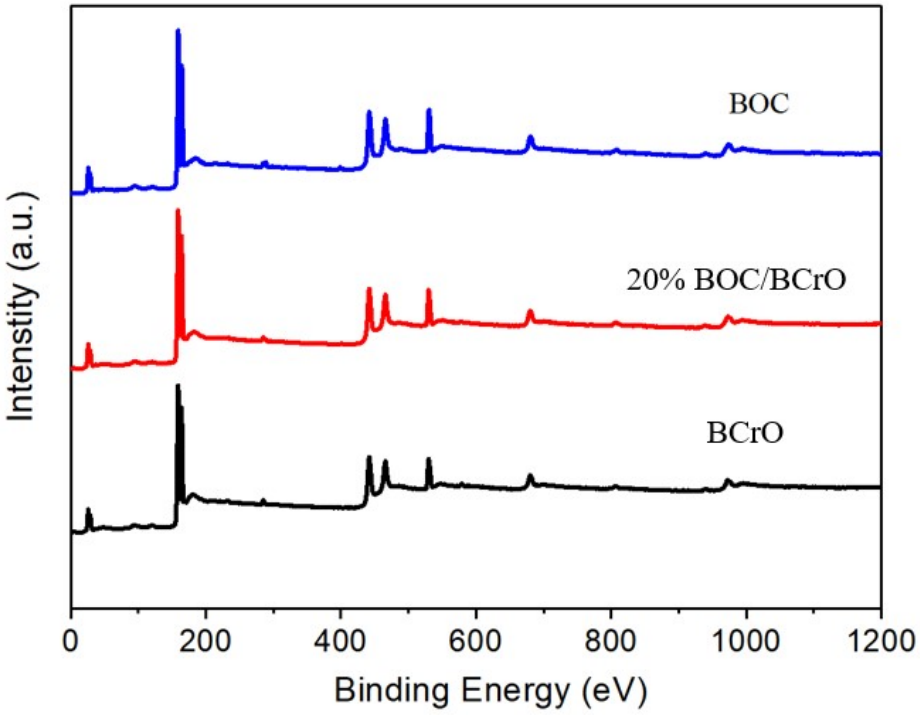

Fig. S2. XPS survey spectra of BOC, BCrO and 20% BOC/BCrO.

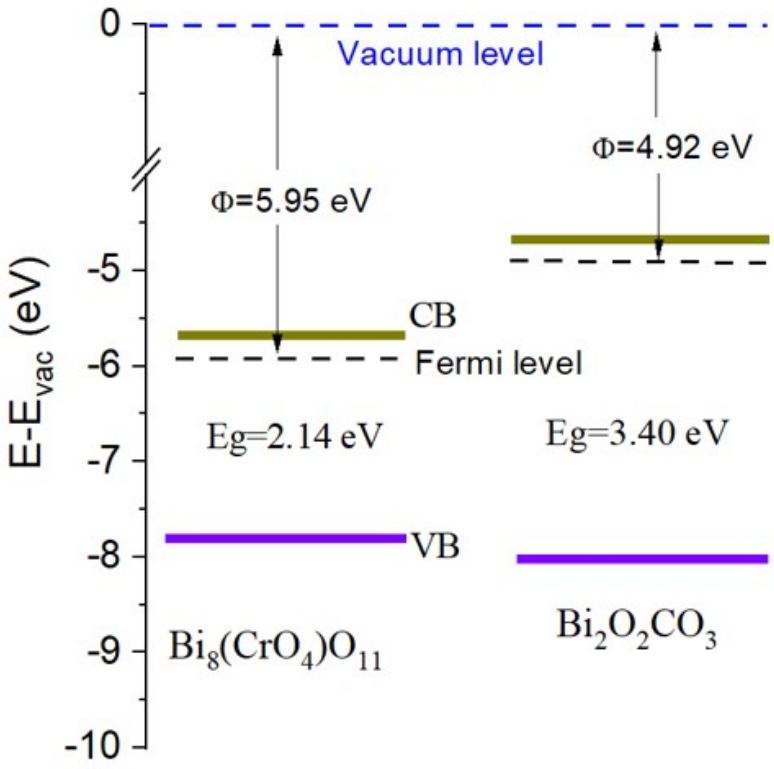

Fig. S3. The estimated energy band diagram.

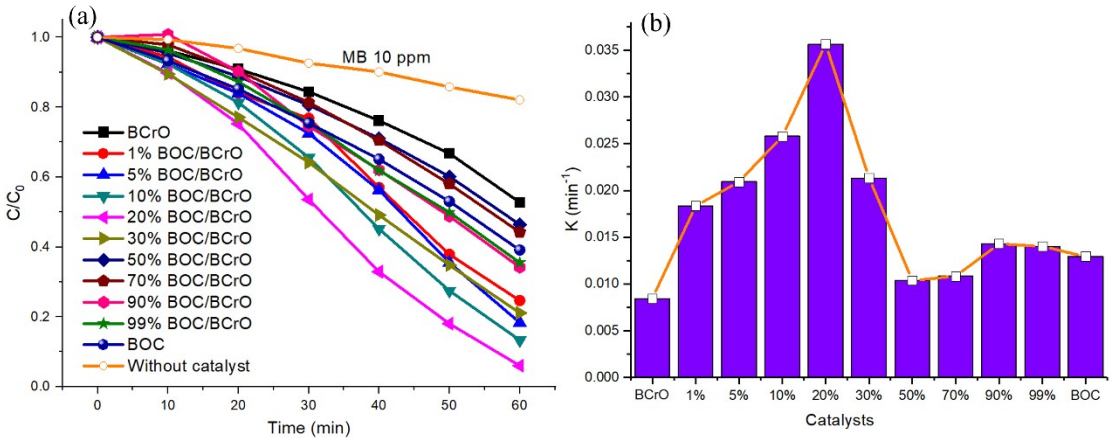

Fig. S4. (a) Degradation efficiency, (b) reaction rate constant of MB (10 ppm) over the prepared catalysts.

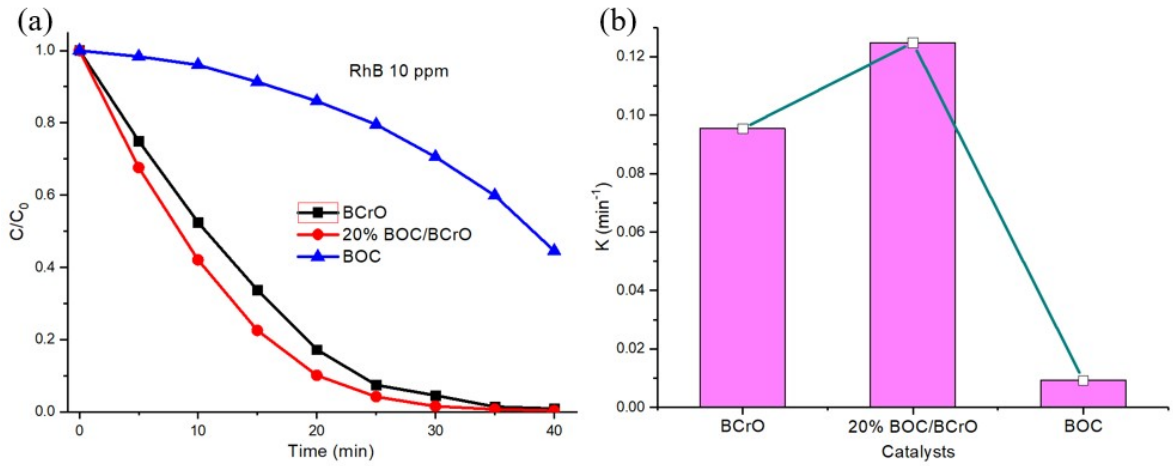

Fig. S5. (a) Degradation efficiency, (b) reaction rate constant of RhB (10 ppm) over the typical catalysts.

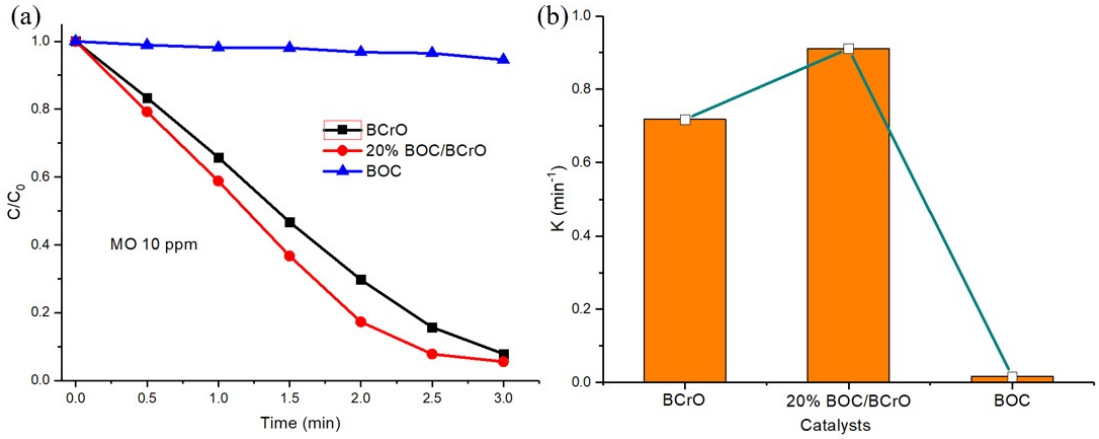

Fig. S6. (a) Degradation efficiency, (b) reaction rate constant of MO (10 ppm) over the typical catalysts.

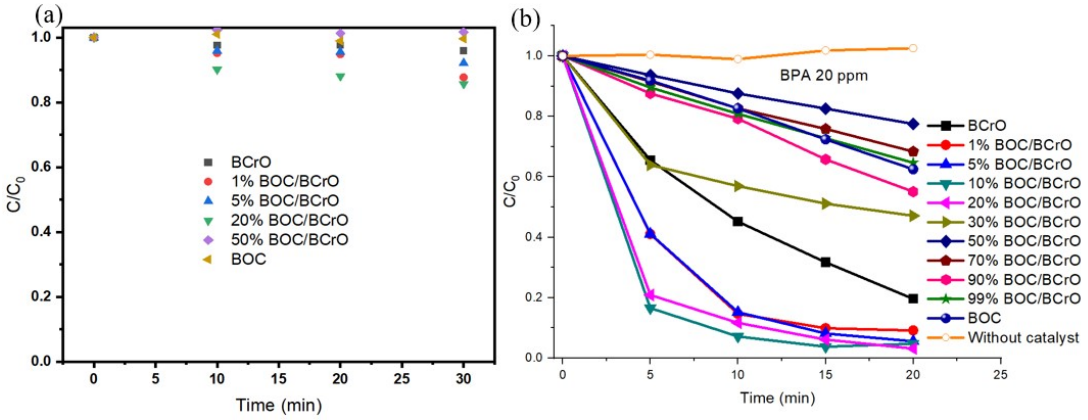

Fig. S7. (a) Adsorption performances and (b) degradation efficiency of BPA (20 ppm) over the catalysts.

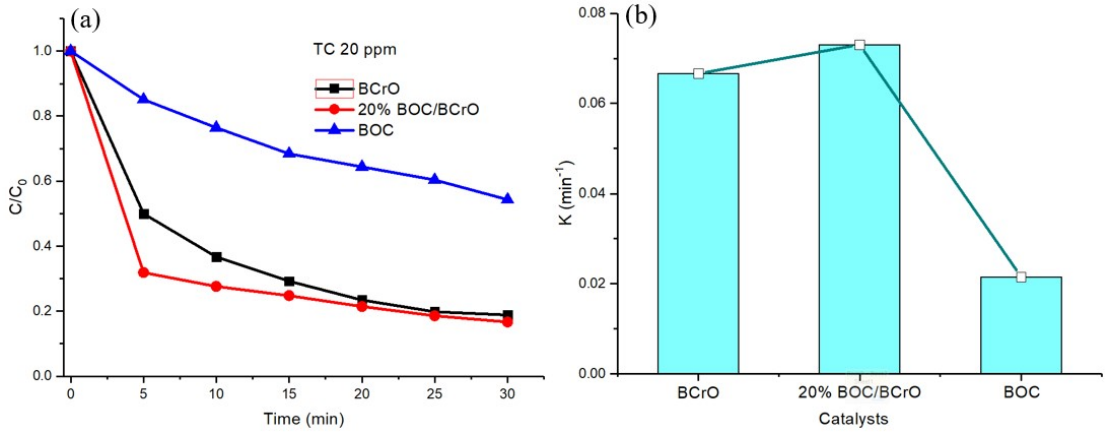

Fig. S8. (a) Degradation efficiency, (b) reaction rate constant of TC (20 ppm) over the typical catalysts.

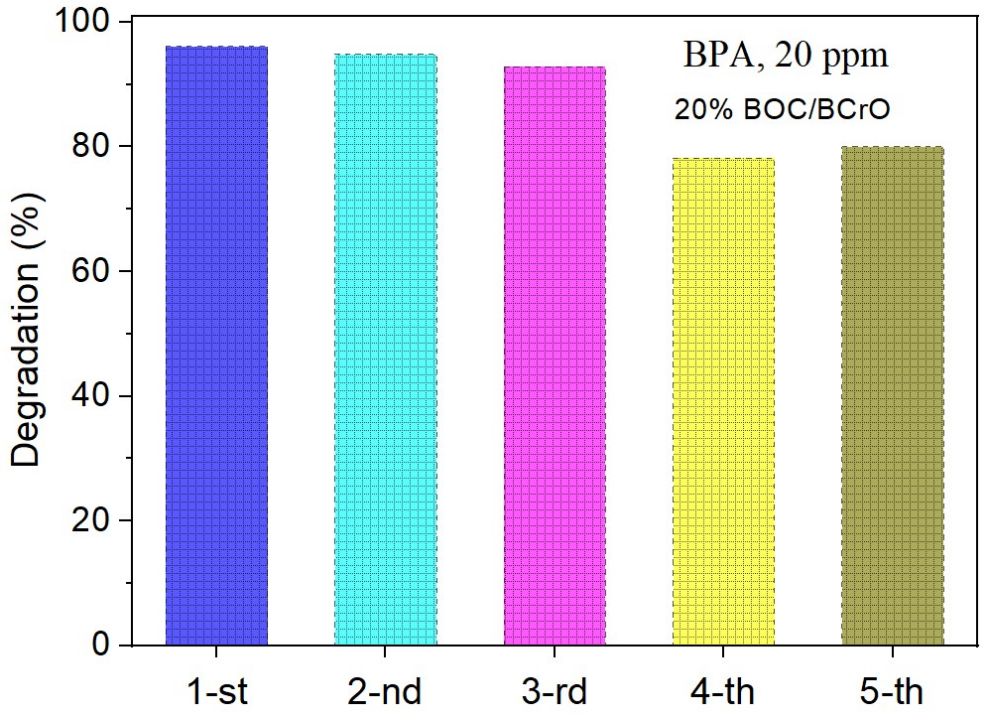

Fig. S9. Cycle curves of BPA over 20% BOC/BCrO heterojunction.

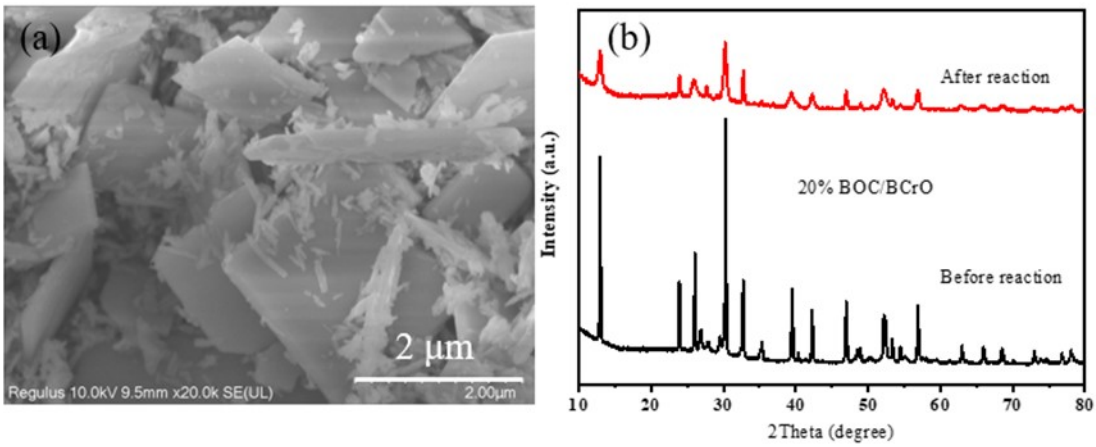

Fig. S10. (a) SEM and (b) XRD of 20% BOC/BCrO after reaction.

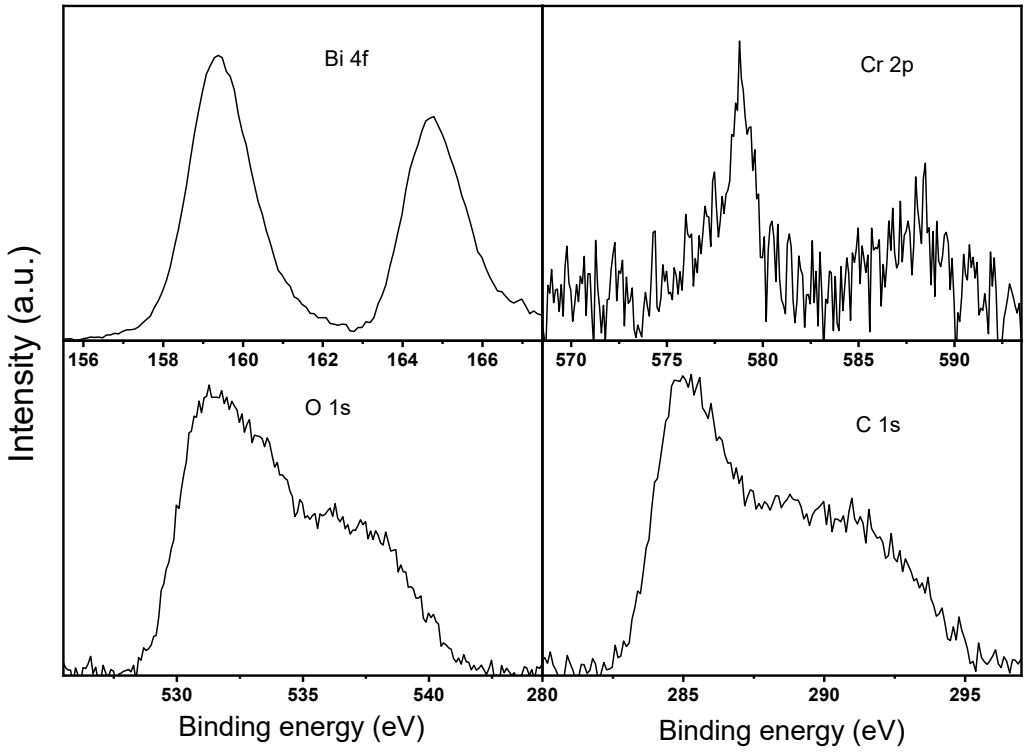

Fig. S11. XPS spectra of 20% BOC/BCrO after reaction.

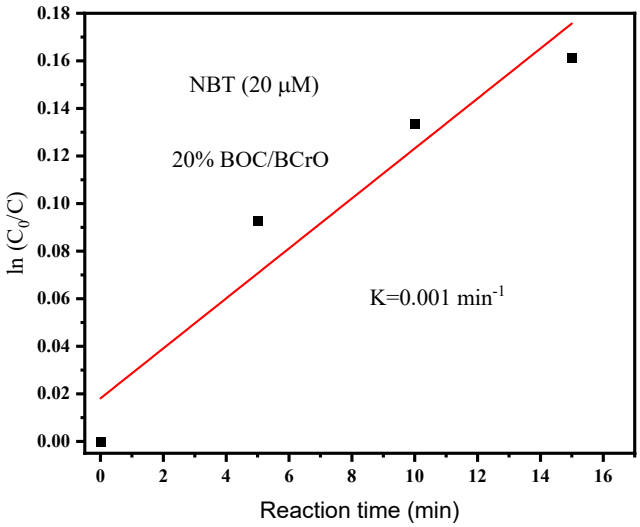

Fig. S12. The kinetic curves of NBT over 20% BOC/BCrO.

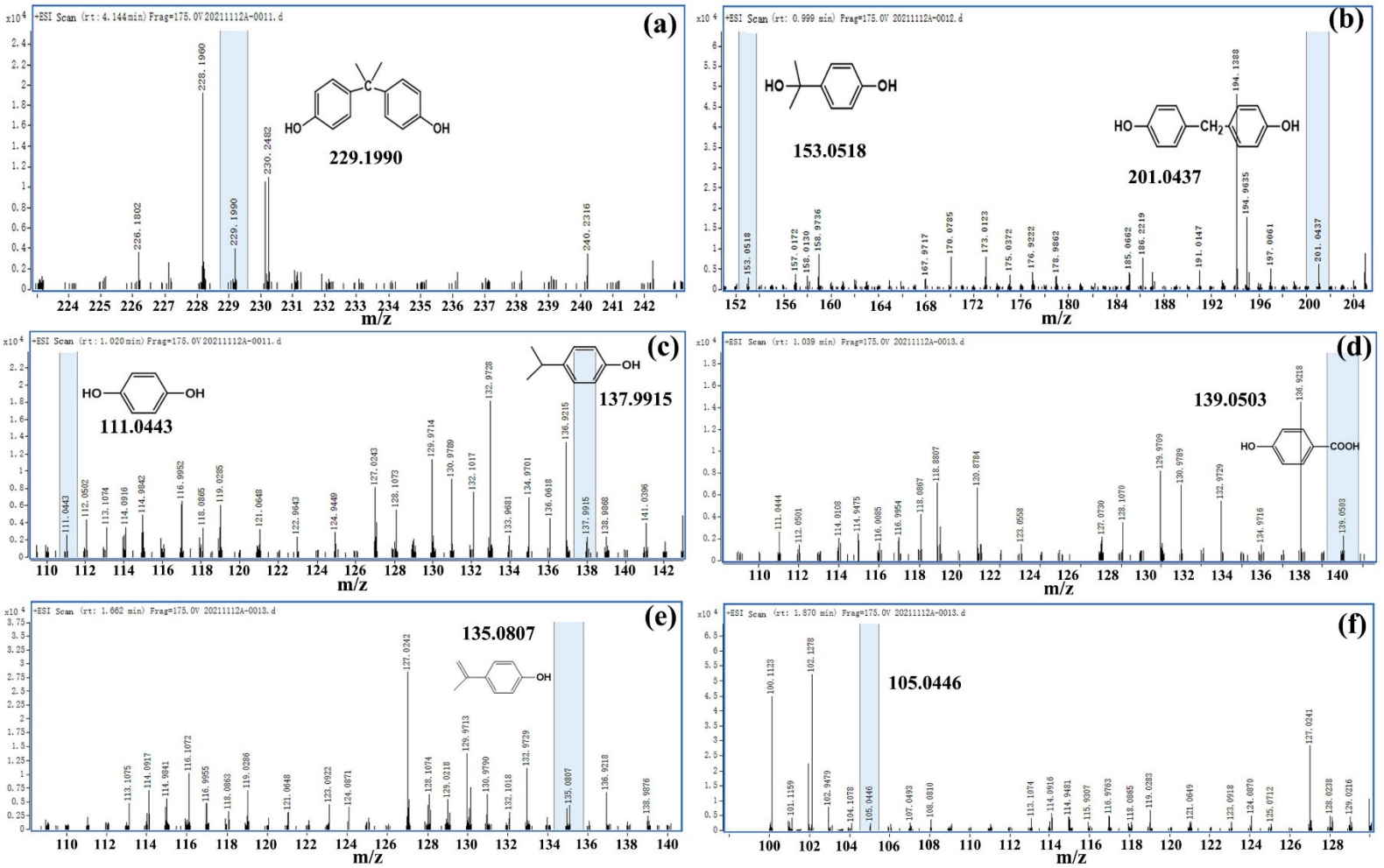

Fig. S13. The mass spectrums of intermediates for BPA degradation.

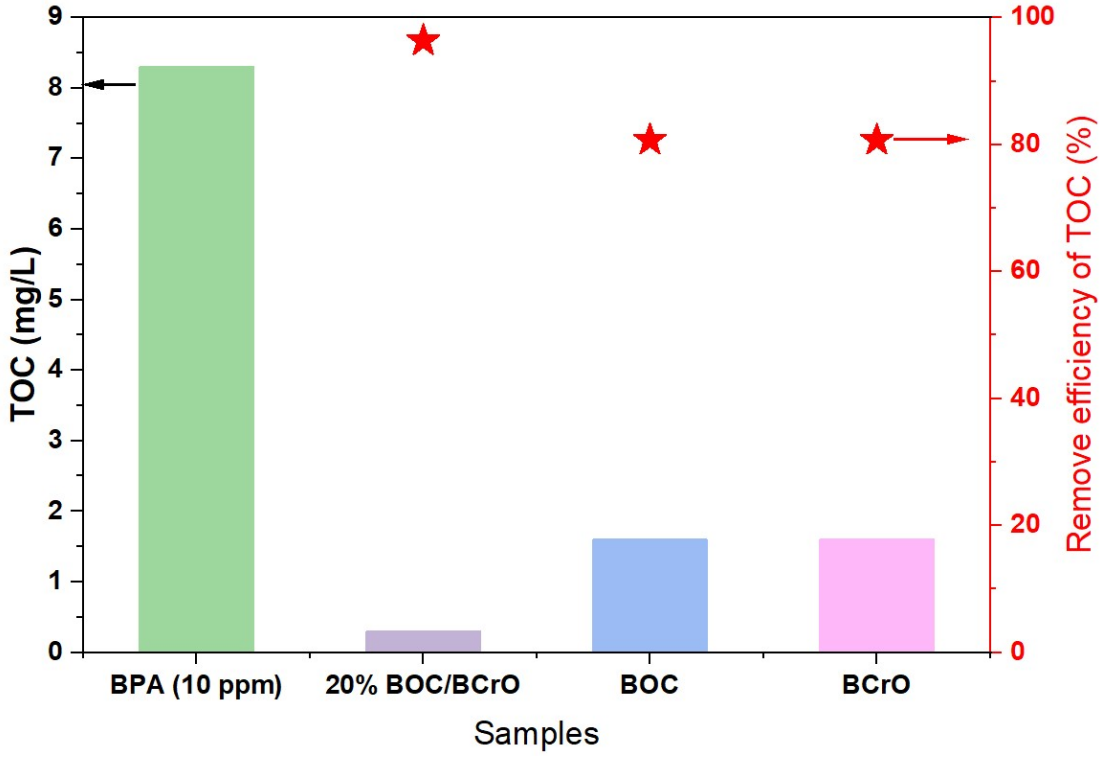

Fig. S14. TOC results of the BPA and its degradation products over the typical catalysts.

The TOC of 10 ppm BPA is about 8.3 mg/L, which is close to the theoretical result (8 mg/L). After reaction, the TOC of 20% BOC/BCrO, BOC and BCrO are about 0.3, 1.6 and 1.6 mg/L, respectively. The corresponding remove efficiencies of TOC are 96.4%, 80.7% and 80.7%, respectively. The results show that 20% BOC/BCrO has the highest photocatalytic activity and almost all BPA can be mineralized into CO_2 and H_2O.

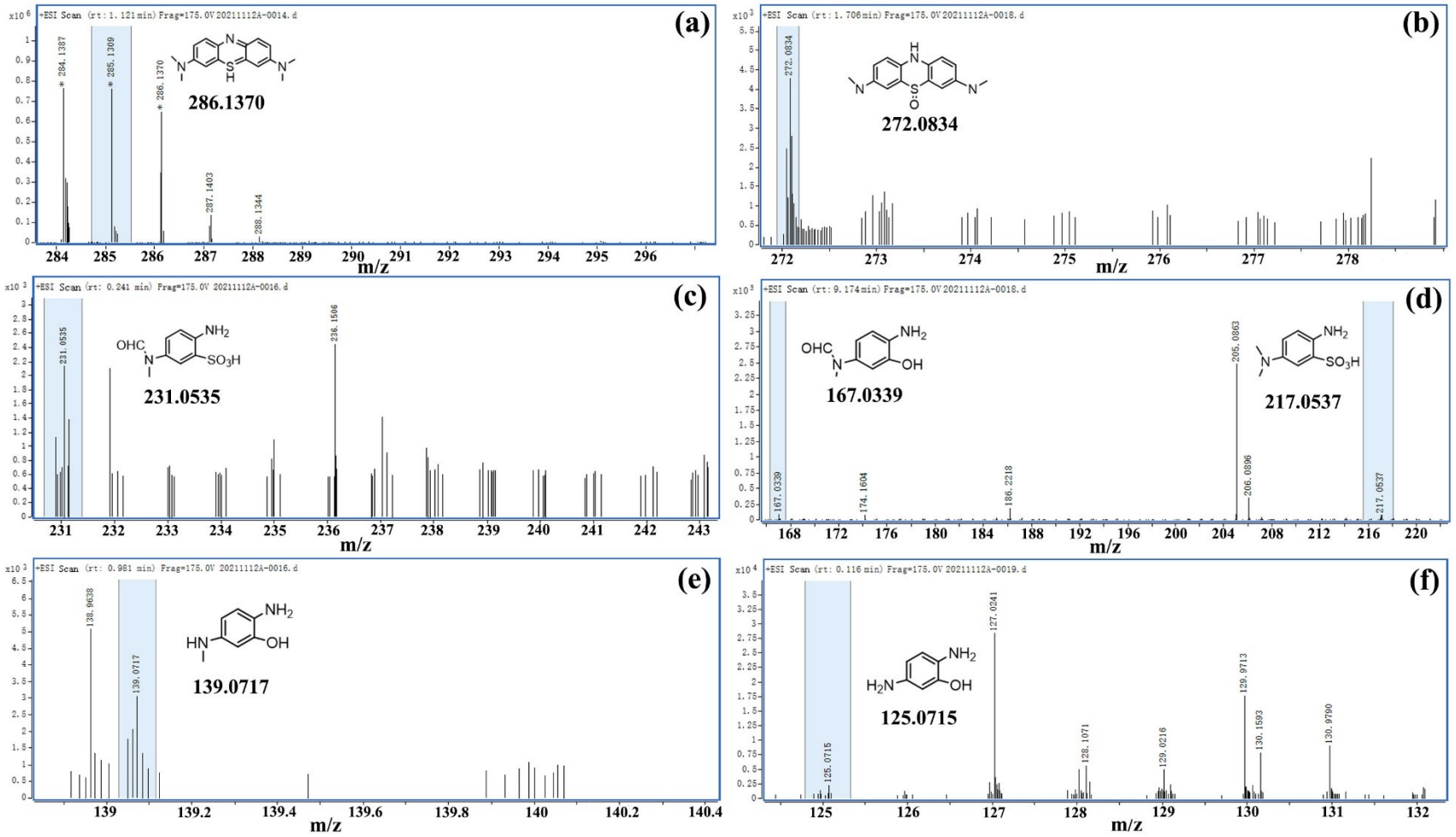

Fig. S15. The mass spectrums of intermediates for MB degradation.

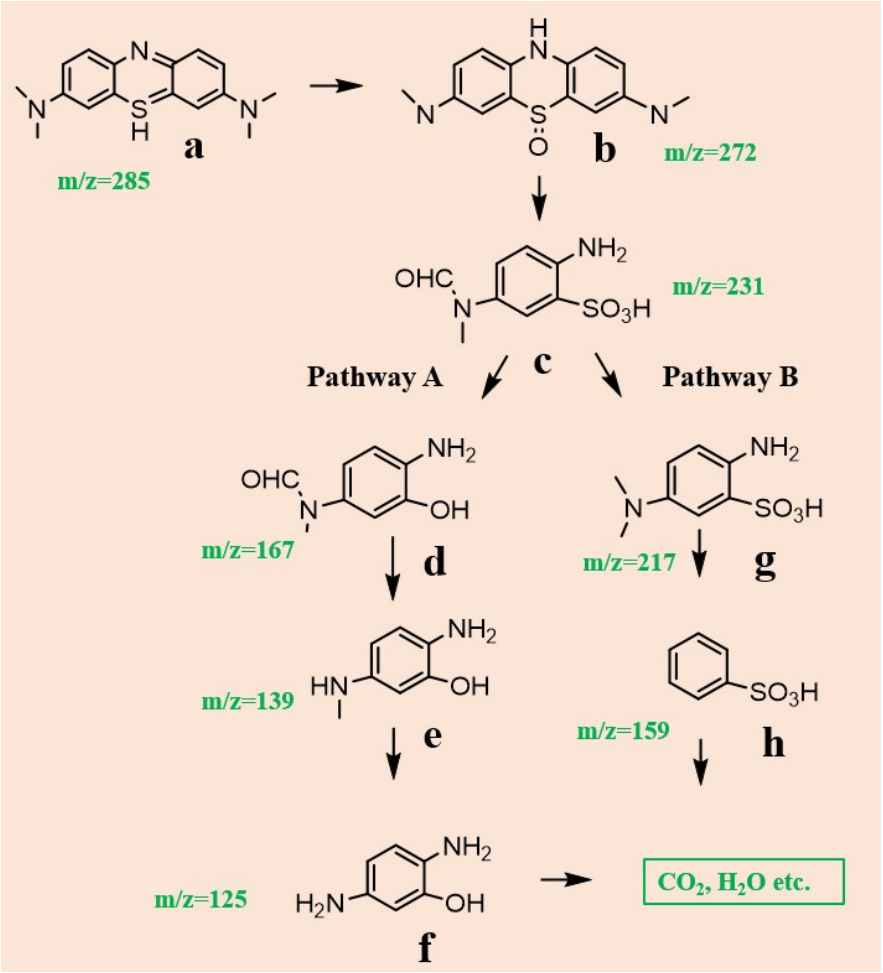

Fig. S16. Proposed photodegradation pathways of the MB in the presence of 20% BOC/BCrO system.

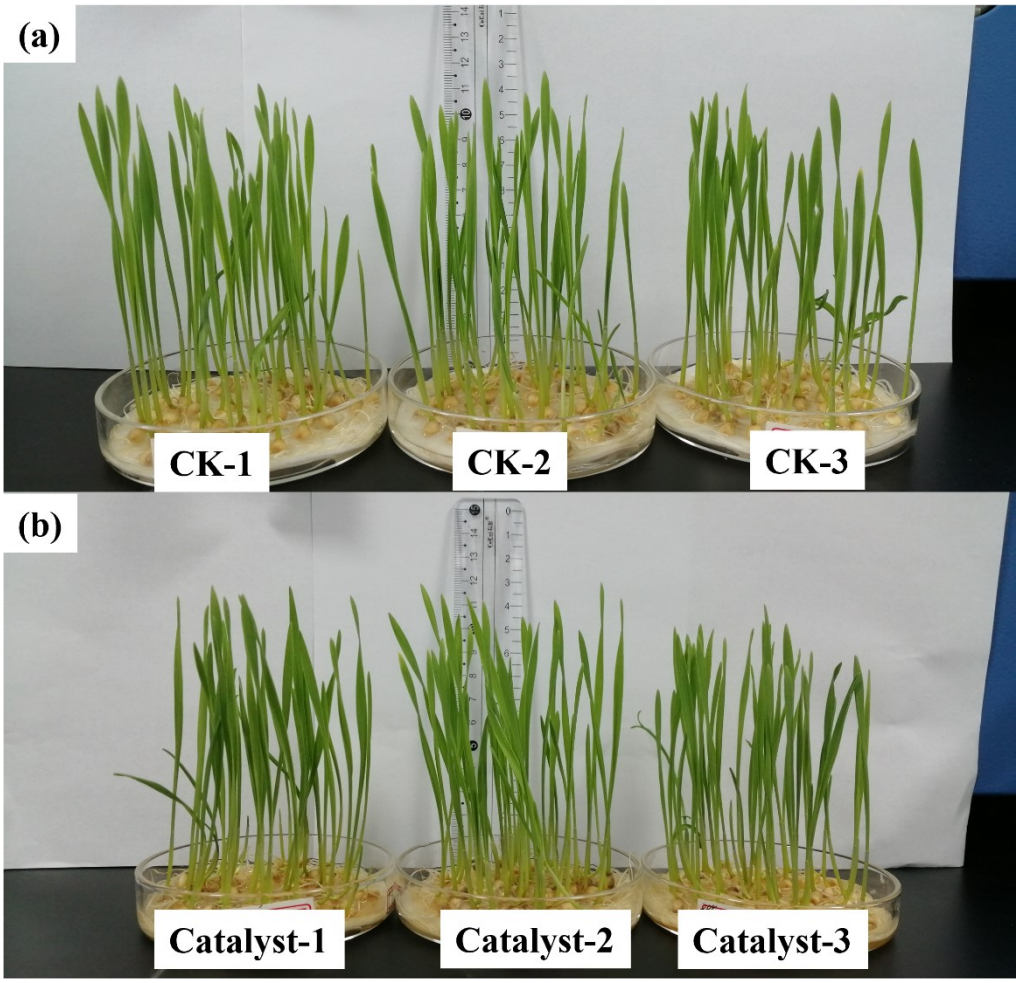

Fig. S17. The growth state of wheat seeds in (a) water and (b) 20% BOC/BCrO after seven-days incubation at 25 ℃.

S1: Al-Kahtani A A, Alshehri S M, Naushad M, et al. Fabrication of highly porous N/S doped carbon embedded with ZnS as highly efficient photocatalyst for degradation of bisphenol. International journal of biological macromolecules, 2019, 121: 415-423.

S2: Yang Y Y, Zhang X G, Niu C G, et al. Dual-channel charges transfer strategy with synergistic effect of Z-scheme heterojunction and LSPR effect for enhanced quasi-full-spectrum photocatalytic bacterial inactivation: new insight into interfacial charge transfer and molecular oxygen activation. Applied Catalysis B: Environmental, 2020, 264: 118465.

S3: Kumar S, Kaushik R D, Purohit L P. ZnO-CdO nanocomposites incorporated with graphene oxide nanosheets for efficient photocatalytic degradation of bisphenol A, thymol blue and ciprofloxacin. Journal of Hazardous Materials, 2022, 424: 127332.

S4: Kim B, Jang J, Lee D S. Enhanced photocatalytic degradation of bisphenol A by magnetically separable bismuth oxyiodide magnetite nanocomposites under solar light irradiation. Chemosphere, 2022, 289: 133040.

S5: Krishnan S, Karim A V, Shriwastav A. Visible light responsive Cu-N/TiO_2 nanoparticles for the photocatalytic degradation of bisphenol A. Water Science & Technology, 2022, 86(6): 1527-1539.

S6: Qin Y, Yang B, Li H, et al. Immobilized $BiOCl_{0.75}I_{0.25}$/g-C_3N_4 nanocomposites for photocatalytic degradation of bisphenol A in the presence of effluent organic matter. Science of The Total Environment, 2022, 842: 156828.

S7: Wen X J, Niu C G, Zhang L, et al. An in depth mechanism insight of the degradation of multiple refractory pollutants via a novel $SrTiO_3$/BiOI heterojunction photocatalysts. Journal of Catalysis, 2017, 356: 283-299.

S8: Yang S F, Niu C G, Huang D W, et al. $SrTiO_3$ nanocubes decorated with Ag/AgCl nanoparticles as photocatalysts with enhanced visible-light photocatalytic activity towards the degradation of dyes, phenol and bisphenol A. Environmental Science: Nano, 2017, 4(3): 585-595.